

3D Printed Spectroelectrochemical Platform for Redox-Based Bioelectronics

Chen-Yu Chen, Eunkyong Kim, Fauziah Rahma Zakaria, Monica J. Chu, Benjamin Wu, Gregory F. Payne, and William E. Bentley*

Redox provides unique opportunities for interconverting molecular/biological information into electronic signals. Here, the fabrication of a 3D-printed multiwell device that can be interfaced into existing laboratory instruments (e.g., well-plate readers and microscopes) to enable advanced redox-based spectral and electrochemical capabilities is reported. In the first application, mediated probing is used as a soft sensing method for biomanufacturing: it is shown that electrochemical signal metrics can discern intact mAbs from partially reduced mAb variants (fragmentation), and that these near-real-time electrical measurements correlate to off-line chemical analysis. In the second application, *operando* spectroelectrochemical measurements are used to characterize a redox-active catechol-based hydrogel film: it is shown that electron transfer into/from the film correlates to the molecular switching of the film's redox state with the film's absorbance increasing upon oxidation and the film's fluorescence increasing upon reduction. In the final example, a synthetic biofilm containing redox-responsive *E. coli* is electro-assembled: it is shown that gene expression can be induced under reducing conditions (via reductive H₂O₂ generation) or oxidative conditions (via oxidation of a phenolic redox-signaling molecule). Overall, this work demonstrates that 3D printing allows the fabrication of bespoke electrochemical devices that can accelerate the understanding of redox-based phenomena in biology and enable the detection/characterization redox activities in technology.

1. Introduction

Information transfer between biological systems and electronic devices has for decades enabled transformative and even life-saving technologies (e.g., implantable cardioverter-defibrillators [ICDs] and automated external defibrillators [AEDs]). A most basic form of communication within electronic devices involves the free movement of electrons within conductive materials; biological systems also employ electron movement to process information, but in biology electrons are carried by molecules and information is transferred within spatially defined redox reactions.^[1,2] The redox communication modality is fundamental in biology and at the same time, enables bidirectional communication with devices.^[3,4] Its study, however, is complex—phenomena are not molecularly specific (e.g., impact of reactive oxygen species) and often occur at interfaces (e.g., membrane potential). Furthermore, its study is hindered by the lack of instrumentation and analytical methodologies that provide fundamental

insight.^[5,6] We believe there are a great many potentially transformative advancements that could be developed if there were better and simpler means to interrogate the redox communication modality in molecular and cellular systems.

In this work, we designed and constructed a simple, 3D printed, spectroelectrochemical sensor/actuator device that employs redox communication to not only detect but carry out advanced functions that have otherwise not been available (Scheme 1). That is, in each of three examples, new biological insights are gleaned owing to the ability to transmit redox-based information to and from these molecular and cellular systems. Importantly, because the electronics are aligned with optical assessments in multiwell plates, the device enables real-time working assessment. We demonstrate the capability of this device with three emerging research topics: i) rapid, parallel electronic assessment of antibody structural integrity; ii) *operando* electrofluorochromic materials analysis; and iii) voltage dependent electrogenetic actuation of gene expression in cells that are electroassembled in polyethylene glycol hydrogels (i.e., a sliding voltage shifts or “programs” gene expression). In each example,

C.-Y. Chen, F. R. Zakaria, M. J. Chu, B. Wu, W. E. Bentley
Fischell Department of Bioengineering
University of Maryland
College Park, MD 20742, USA
E-mail: bentley@umd.edu

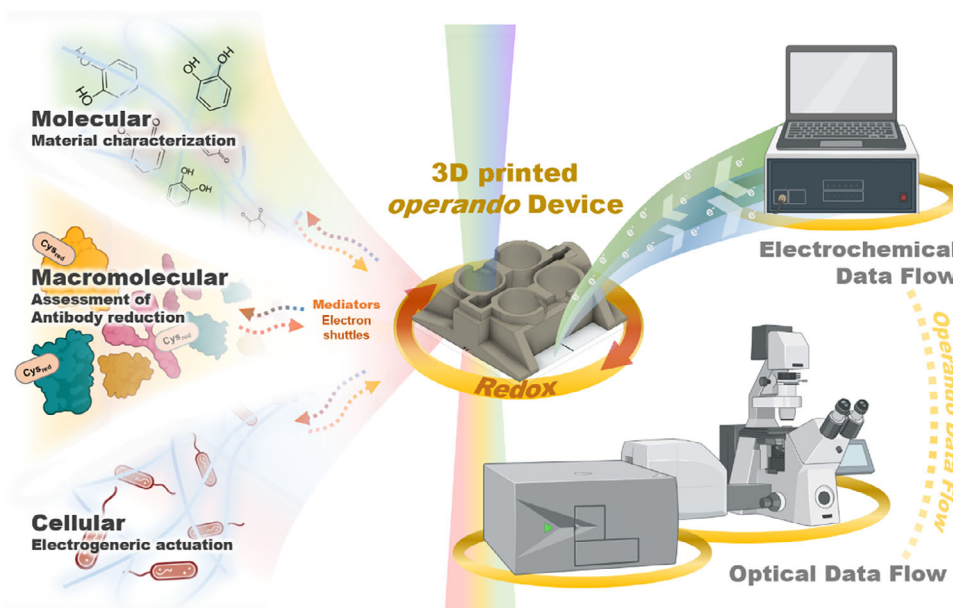
C.-Y. Chen, E. Kim, F. R. Zakaria, M. J. Chu, B. Wu, G. F. Payne, W. E. Bentley
Institute for Bioscience and Biotechnology Research
University of Maryland
College Park, MD 20742, USA

C.-Y. Chen, E. Kim, F. R. Zakaria, M. J. Chu, B. Wu, G. F. Payne, W. E. Bentley
Robert E. Fischell Institute for Biomedical Devices
University of Maryland
College Park, MD 20742, USA

 The ORCID identification number(s) for the author(s) of this article can be found under <https://doi.org/10.1002/smt.202401843>

© 2025 The Author(s). Small Methods published by Wiley-VCH GmbH. This is an open access article under the terms of the [Creative Commons Attribution-NonCommercial-NoDerivs](#) License, which permits use and distribution in any medium, provided the original work is properly cited, the use is non-commercial and no modifications or adaptations are made.

DOI: 10.1002/smt.202401843



Scheme 1. The multiwell spectroelectrochemical modular system.

we have detailed investigate the performance of this system and its potential for other appealing scientific questions.

By using this simple 3D printed device that communicates via the redox communication modality, we are in a better position to reveal unexplored scientific cues and convert them directly into processable digital formats via electrochemical and optical pathways. One can take advantage of programmable electronic inputs to trigger molecular, optical, and other reactions via this interface. The universal modular design, combined with its transparent and electrochemically conductive electrode materials, offers an opportunity to use as an insert to common laboratory electrochemical and optical analytical equipment for multidirectional exchange of electrical, chemical, and optical information, as well as *operando* data collection.

2. Results

2.1. Fabrication of a Multiwell Spectroelectrochemical Sensor/Actuator Device with a Docking Station

We constructed a multiwell ITO-based electronic device and a docking station (Figure 1) for simultaneous and dynamic electrochemical and optical interrogation, and actuation of samples. The system uses a three-electrode setup, including shared reference and counter electrodes and a customizable working electrode, providing an operating interface that enables bidirectional information transfer in real time. In Figures 1A and S1 (Supporting Information), a multiwell 3D-printed housing is positioned on top of transparent ITO electrodes. As noted above, we use ITO for enabling simultaneous optical and electrochemical measurement. Also, we have found that particularly for redox assessments with sulfhydryls, ITO exhibits less fouling characteristics than gold as an electrode material (see Figure S2, Supporting Information). By design, the bottom surface area of the 3D-printed wells determines the area of the bottom working electrode. The

central well provides for an agarose salt bridge that is shared by neighboring wells, facilitating ion transport between the working, counter, and reference electrodes. We have created both 4- and 8-well models suiting different applications. Figure 1B depicts the design and fabrication workflow (see the Experimental Section), resulting in a construction that provides for simple sample loading, monitoring (i.e., optically clear), and sample manipulation, should reagents or materials need to be added. As depicted in the right panel of Figure 1B, a docking station was developed to facilitate adaptation to conventional optical/electrochemical analyzers, both sample wells and docking station were designed with the same dimensions as a conventional 96-well plate. In this way, our device can be deployed as simple insert into commercial spectrophotometers. Finally, to evaluate electrochemical performance, stability, and assembly quality, we loaded solutions with redox mediator, ferricyanide ($K_3Fe(CN)_6$), in all sample wells. We then performed cyclic voltammetry (CV) on each, consistently revealing insignificant relative standard deviations for both the 4- and 8-well devices (1.76% and 4.95%, respectively) (Figure S3A, Supporting Information).

2.2. Rapid Detection of Redox-Mediated Monoclonal Antibody (mAb) Fragmentation

Efficacy of antibody therapeutics depends on their three-dimensional structure. In turn, structure is strongly dependent on not only the primary sequence, but the microenvironment surrounding each molecule wherein solvents and reactive molecules or residues can modulate assembly. That is, antibody manufacture, typically using recombinant Chinese hamster ovary (CHO) cells, can result in a variety of redox modifications (e.g., disulfide reduction).^[7,8] Cysteine residues, for example, are critically important and redox active. Their sulfhydryl groups, when oxidized, form the basis for intra- and interchain

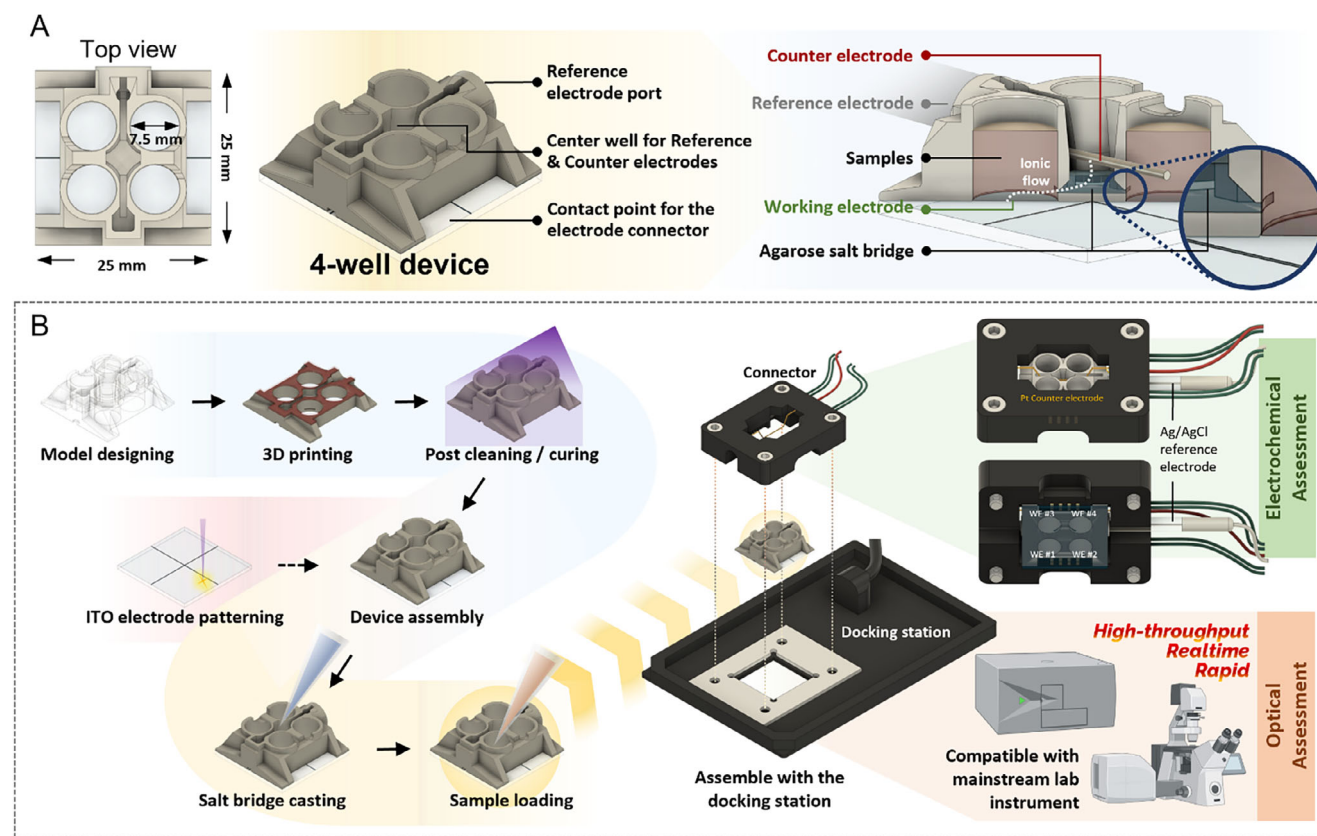


Figure 1. Fabrication of the testing platform using customizable 3D printed housing coupled with transparent patterned ITO electrodes. A) The 3D printed housing with sample wells and a central salt bridge well located on the top of the ITO electrodes. The central salt bridge facilitates ionic transport and electron flow. B) A 3D CAD model was initially designed using CAD software and prints were fabricated using LCD resin 3D printers. Several methanol rinses were applied to remove uncured resin. Prints were then post-cured in a UV box to attain maximum structural strength. Meanwhile, the ITO-coated glasses were patterned using a carbon dioxide laser engraver to generate electrodes that align with the wells in the 3D printed housings. UV glue was used to bind the 3D printed housings and the patterned ITO electrodes. Once the device assembly is completed, the electrode area becomes well-defined by the cross-section area of the wells. An agarose gel was then cast in the middle chamber which later served as the salt-bridge that connected all four wells. When connected to the docking station, the ITO electrodes are individually controlled by the electrochemistry analyzer. The electrode connector is equipped with a platinum wire that serves as the counter electrode. When assembled with the ITO device, the counter electrode immerses into the salt bridge and completes the electrochemical circuit. The dimensions of the system were designed to adapt as an insert to general lab optical and electrochemical instruments.

linkages that establish and maintain structure.^[9] Importantly, both upstream and downstream processes can result in such antibody structural fragmentations via interchain disulfide bond reduction.^[10] In addition, there is a paucity of process analytical technologies that are used for optimizing or even correcting antibody manufacturing processes in real time.^[10] In our first demonstration, we sought to provide a straightforward yet reliable electrochemical tool that enabled access to redox-based alterations, specifically disulfide reduction, to be conveyed directly into digital signatures that, in turn, could be used rapidly, at low cost, and without complex instrumentation. Here, we intentionally provide redox mediators (i.e., weak oxidant, 1,1'-ferrocenedimethanol, Fc) to samples to probe the mediator accessible redox activity (MARA).^[10] That, in turn, enable “programmed” electron transfer between electrodes and antibodies. We refer to this method for detecting the redox character of samples as “mediated electrochemical probing” (MEP) (Figure 2A).^[10]

Here, we demonstrate the electrochemical characterization of mediator-accessible cysteine, which is a well-characterized redox-sensitive molecular “switch” in biological systems. When antibodies undergo reduction (i.e., mAb fragmentation), including disulfide bond disruption, there is a corresponding increase of cysteine thiol groups. As a result, smaller IgG variants (Heavy-Heavy, Heavy-Light, Heavy, and Light chain forms) that have exposed free thiol groups are present in the samples (Figure 2B).

We exploit the redox properties of the exposed thiol groups to characterize the reduction and disassembly of antibodies. In Figure 2C, the mediator, Fc, works as a messenger shuttling the electrons from the free thiols of the reduced antibodies to the electrode. Specifically, on the left, oxidized Fc interacts with the free thiol groups to capture electrons.^[11,12] This reduces Fc, which is then reoxidized at the electrode, enabling redox cycling.^[10] In this way, oxidation of the cysteine’s thiol is amplified and easily recorded. At the right of Figure 2C, oxidized Fc is reduced at the electrode, which depletes its concentration and ability to

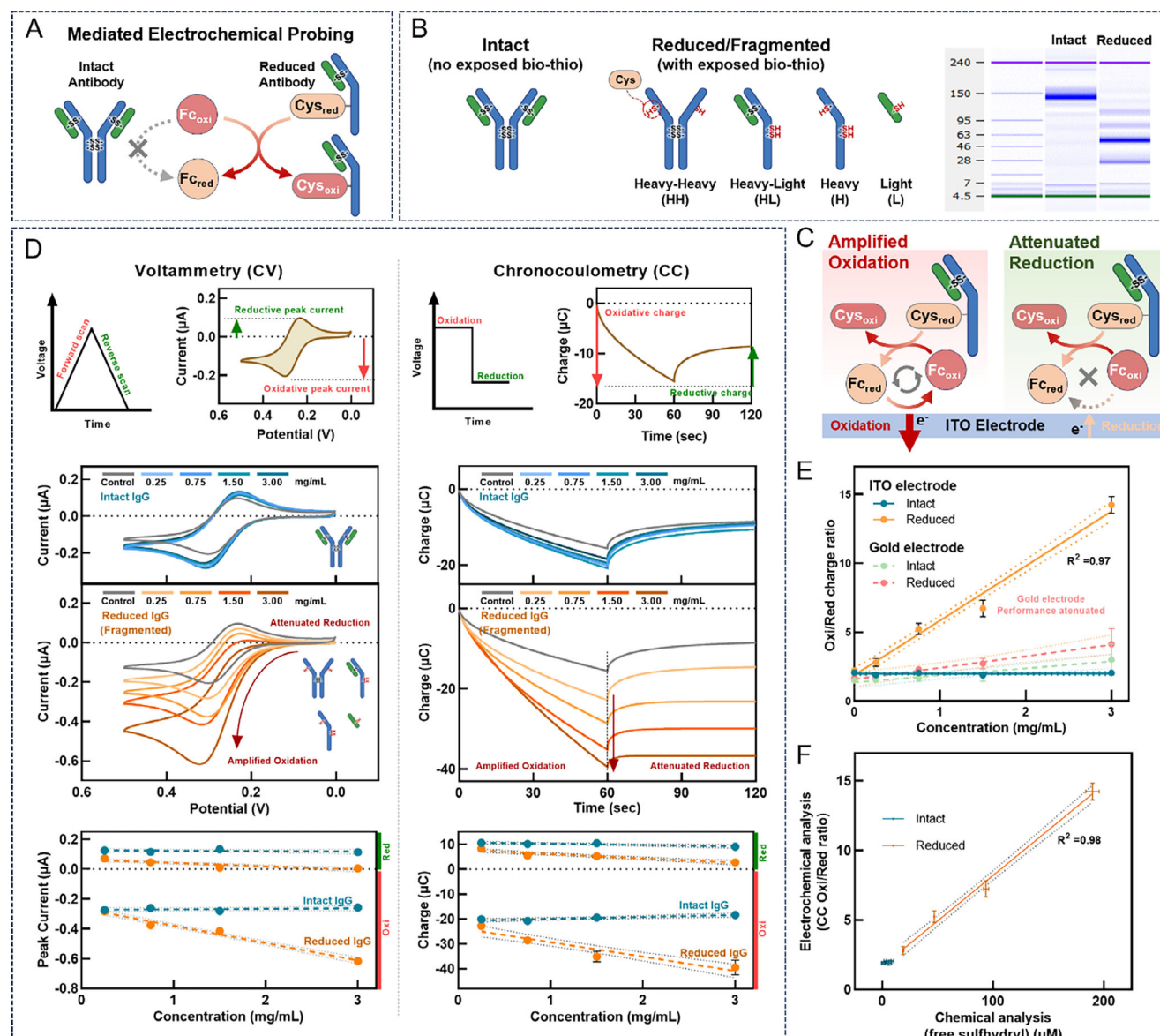


Figure 2. Direct electronic assessment of antibody structure (reduction) via mediated electrochemical probing. A) Mediated electrochemical probing (MEP) uses redox mediator, ferrocene (Fc), to discriminate intact antibody from its reduced fragments. The exposed thiols on the reduced fragments are oxidized by Fc_{oxi} , while the same reaction cannot be triggered with intact antibody due to the lack of free thiols. B) When antibody reduction occurs, the sulfhydryl concentration increases along with the number of reduced fragments, as confirmed by CE. C) Fc works as a messenger that carries the structural information correlated to the disulfide bond reduction to the ITO electrode and converts it into a digital signature. At the electrode, the excessive Fc_{red} can amplify the oxidation and attenuate the reduction reactions. D) In CV, applied potential is varied spanning Fc oxidation and reduction regions while CC offers a step switching between constant oxidative and reductive potentials. For CV, the oxidative and reductive peak currents ($i_{\text{peak,oxi}}$ or $i_{\text{peak,red}}$) are defined as the minima and maxima in the peak currents, respectively. For CC, the oxidative charge (ΔQ_{oxi}) is defined as the change in charge during the first 60 s, while the reductive charge (ΔQ_{red}) is defined as the change in charge during the second 60 s. When testing reduced IgG, both CV and CC results show clear amplification on oxidative peak current ($R^2 = 0.97$) and oxidation charge ($R^2 = 0.84$), with the attenuation on reductive peak current ($R^2 = 0.77$) and reduction charge ($R^2 = 0.83$). Meanwhile, both CV and CC show no significant differences when IgG is intact, reflecting lack of Fc-reactive cysteine thiols. E) The oxi/red charge ratio, as indicated, using ITO electrodes serves as a powerful indicator of the total free thiols in the sample. F) Electrochemical results are consistent with the free sulfhydryl using Ellman's assay ($n = 3$).

react with the mAb sulfhydryl, effectively attenuating the reduction current. In Figure 2D, we show two electrochemical methods with distinct voltage input schemes, CV or chronocoulometry (CC) for solutions containing redox mediator, Fc. For CV, we mixed Fc (to 50×10^{-6} M) with IgG (0.25, 0.75, 1.5, and 3 mg

mL^{-1} final concentrations). As described in the Supporting Information, we intentionally reduced the purchased IgG with Tris(2-carboxyethyl)phosphine (TCEP) to obtain known quantities of reduced mAb fragments. In this way, known mixtures of samples could be tested using MEP. In samples of intact IgG (upper

panel), there were no differences observed between the Fc controls and Fc/intact IgG mixtures, indicating no interaction between Fc and intact IgG. However, when tested samples with reduced IgG, we discovered oxidative current amplification and reductive current attenuation at the peak potentials (middle panel). We further discovered that both the increase in the oxidative current and the decrease in reductive current corresponded to the increase of total exposed biothiol content in the IgG samples. That is, as the concentration of reduced forms was increased, we observed a linear decrease in the oxidative peak and the attenuation of the reductive peak (lower panel). Interestingly, the changes were most dramatic in the oxidative peak, which was amplified several fold as the concentration of reduced IgG was increased to 3 g L^{-1} . Almost identical results were obtained for the CC measurements. The similar results of CV and CC measurements demonstrate that the electronic input was conveyed from the device to the sample and then quantified in a robust manner—the conveyance of electrons to and from the samples via the Fc was consistent. We subsequently calculated the ratio of the oxidation and reduction charge and found that the ITO electrodes outperformed gold electrodes (Figure 2E), likely owing to the fouling of gold during sulfhydryl oxidation (Figure S2, Supporting Information). In addition, we investigated the impact of scan rate on the sensitivity and signal-to-noise ratio of free biothiol detection (Figures S5 and S6, Supporting Information). We found that our method can statistically discriminate intact/reduced mAb even at higher scan rates (10 mV s^{-1}).

Finally, we characterized our MEP methodology to the chemical assay (Ellman's assay) which quantifies sulfhydryls based on a chemically modified colorimetric label (Figure S7, Supporting Information). We found (Figure 2F) a direct linear relationship between the MEP methodology using our device and the standard Ellman's assay. Moreover, because the device is fabricated so that four or eight measurements can be obtained simultaneously, our method provides for rapid assignment of statistical significance for a number of samples. In sum, our electrochemical platform offers a rapid, robust, and reproducible method for accurately representing reduced antibody information (antibody fragmentation) that is essential for ensuring quality control in biotherapeutic development and biopharmaceutical manufacturing.

2.3. An Operando Technique for Electrofluorochromic Materials Characterization

Electrofluorochromic materials represent an innovative category of smart materials that exhibit reversible dynamic changes in color or opacity and fluorescence in response to applied electrical cues.^[13,14] These materials have attracted significant interest due to their unique optical properties and diverse applications across various industries, such as energy, electronics, and healthcare. For example, in the energy sector, energy-efficient smart glass^[15] can modulate the transmission of light and heat, reducing the power consumption for temperature control. Other applications including flexible transparent displays,^[16] bioimaging,^[17] biosensor,^[18] and data storage devices^[19] are facilitating the development of a more sustainable world. Interestingly, the optical properties of these materials are correlated

to redox state transitions. The ability to assess in real-time, the optical and electrochemical properties of these materials will offer invaluable insights into their intrinsic electron transfer processes. That is, there is a growing demand for practical analytical *operando* measurements in understanding the fundamental mechanisms of these electrochromic reactions.^[20,21] Because of its electrical conductivity and optical transparency, ITO has become one of the most widely used materials for working electrodes in spectroelectrochemistry-based biosensors and *operando* measurements,^[22–24] including in our recent report of a method for proline-selective electrochemiluminescence (ECL) from single amino acid protein variants.^[25] Here, we demonstrate how our device offers comprehensive information for electrofluorochromic materials characterization.

Our prior work has demonstrated the manipulation of redox-associated color changes in biomaterials such as chitosan and melanin (e.g., catechol-modified chitosan films),^[26] where we developed means for establishing device memory which can store redox information into the catechol grafted into the chitosan hydrogel through the redox-cycling reaction with mediators.^[26–33] While high-throughput experimentation (HTE) enables simultaneous optical monitoring of multiple target samples due to electronic inputs,^[34] in this study, we leveraged the transparency of ITO in a spectroelectrochemical format for visualizing optical changes at the same time as capturing redox state switching. Our 3D-printed device enables high-throughput operation for in situ and *operando* functionality.

To create a functional material that exhibits redox state switching and “programmed” optical properties, we electroassembled a polyethylene glycol (PEG) hydrogel onto gold and indium tin oxide electrodes. Polyethylene glycol is widely used in pharmaceuticals,^[35] tissue engineering,^[36] and green chemistry^[37] for its ability to work as a coating, support, and even catalyst. Its formation into a hydrogel starts from the polymerization of PEG monomers with reactive terminal functional groups such as thiolates, amines, and maleimides. Notably, a thiolated PEG could be crosslinked using redox mediators (e.g., pyrocyanin [PYO], catechol [CAT], 1,1'-ferrocenedimethanol [Fc],^[38] potassium hexachloroiridate [Ir], and acetosyringone [AS]). The resultant polymer can be further functionalized depending on the mediators or doping materials, yielding unique optical signatures or electrochemical features. For example, catechol enables crosslinking and also confers electrochemical and colorimetric features.^[26,27,30] Catechol-based materials (e.g., catechol-chitosan and catechol-PEG) have been reported to have unique absorption spectra depending on its oxidation/reduction status.^[26,27,32] Here, a thiolated PEG monomer was prepared in buffer ($100 \times 10^{-3} \text{ M}$ PB, pH 7.4) containing catechol ($50 \times 10^{-3} \text{ M}$) to facilitate the polymerization by electrode-based oxidation of the thiol groups at the terminals of the 4-arm monomers into disulfide bonds. When an oxidative voltage is applied, the cross-linked catechol-PEG polymer forms a thin but uniform hydrogel layer on the ITO electrode (Figure 3A). In Figure 3B, we utilized the ITO device and deposited PEG (well No. 1) and catechol-PEG (well Nos. 2–4) by applying a +0.8 V potential for varied deposition times (30, 45, and 60 s) to wells No. 2, No. 3, and No. 4, respectively. As illustrated in Figure S8 (Supporting Information), the charges delivered from the electrode during the 30, 45, and 60-s intervals were 38, 45, and 57 mC, respectively. We found they

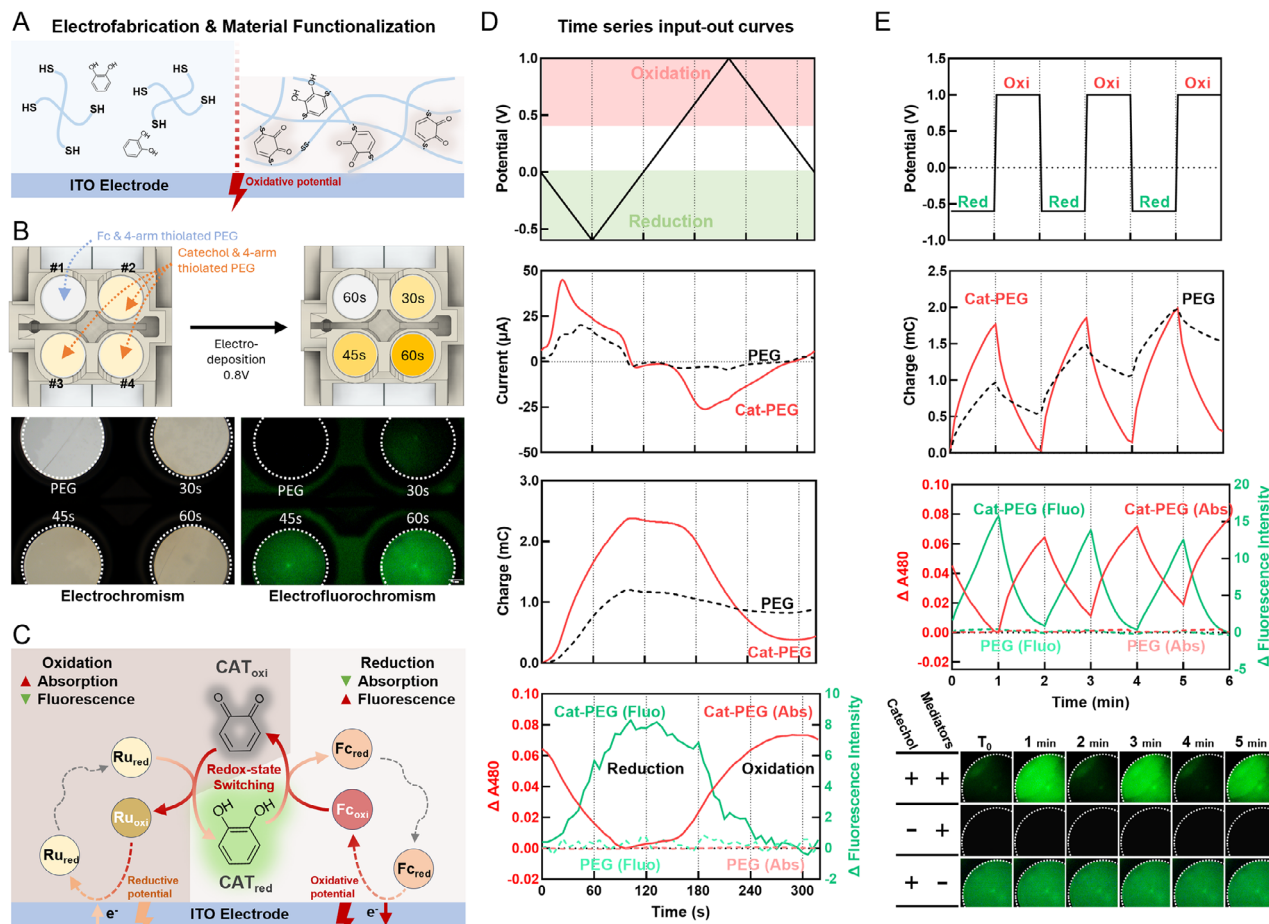


Figure 3. Electroassembled catechol-PEG hydrogel and its electrochromic and electrofluorochromic characteristics. A) Catechol played an important role in the formation of this functionalized biomaterial. The oxidative power provided from the ITO was delivered to the PEG-thiols via catechol oxidation, diffusion, and reaction with PEG. When covalently conjugated to the PEG network, the catechol/quinone further functionalizes the hydrogel enabling redox switching. Its polymerization also enabled the electrochromic and electrofluorochromic features that allows for the color and fluorescence changes corresponding to the redox state of the material. B) The increase of UV-vis absorbance aligns with the increase of deposition charge. Catechol-PEG has an excitation peak at 436 nm and an emission peak at 516 nm. The color and fluorescence across all tested groups could be simultaneously monitored under the microscope. The functionalized catechol-PEG shows clear differences compared to the PEG control. C) Fc and Ru were used to manipulate the redox status of the catechol within the hydrogel. Fc can be oxidized at the electrode and then oxidize the catechol, while Ru can be reduced at the electrode and then reduce the quinone. D) Time-series response curves from input potential sweep using an Fc-Ru mediator pair. The UV-vis absorbance and the fluorescence oscillated 180° out of phase. E) The dynamic responses in fluorescence and colorimetric changes when CC were applied in repeated increments.

were highly correlated to the time over which oxidative potential was applied. Moreover, we found at longer times the hydrogel became darker, presumably owing more cross-linking reactions between catechol-PEG such as in melanin formation.^[32] Because our device is built as a simple modular insert system, we measured both the absorbance spectrum as well as the fluorescence excitation and emission spectra when our device was loaded into a conventional microplate reader. We observed a significant absorbance increase between 400 and 500 nm, suggesting an increase in the number of oxidized catechol molecules,^[26,32] but surprisingly, we also found a unique fluorescence signature. The fluorescence spectrum revealed that catechol-PEG exhibits an excitation peak at 436 nm and an emission peak at 516 nm (Figure S8C, Supporting Information). This suggested that catechol-PEG was not only electrochromic but also electrofluorochromic. We

then placed the docking station under the fluorescence microscope for both colorimetric and fluorescence imaging and imaged all four wells (Figure 3B). We noticed that the darkening of the gel and the fluorescence intensity were both highly correlated to the thickness and the brown color of the catechol-PEG. Moreover, these phenomena occurred within the window of 30–60 s of electrofabrication. Meanwhile, as the negative control, the PEG hydrogel with no catechol exhibited neither a color change nor fluorescence.

2.4. Optical Signatures of Redox-Active Catechol-PEG Hydrogel

As demonstrated previously,^[26,27,30,31,33] the optical properties of the catechol moieties of catechol-conjugated hydrogels vary with

redox state. As illustrated in Figure 3C, two mediators are used to manipulate the redox status of catechol-PEG. Specifically, Fc can be oxidized at the working electrode while hexaammineruthenium(III) chloride (Ru^{3+}) can be reduced. When coupled, oxidized Fc and reduced Ru^{3+} can shuttle an electrical signal applied at the ITO working electrode to further oxidize or reduce the catechol, respectively. Here, we measured the optical responses (both UV-vis absorption and fluorescence emission) depending on the mediators' redox-state switching. Specifically, we used a solution containing two redox mediators (0.2×10^{-3} M of Fc and 0.5×10^{-3} M of Ru^{3+}) to switch the redox state of the catechol-PEG and collected time-dependent absorption (at 480 nm) and the fluorescence data ($\lambda_{\text{emission}}$ @ 520 nm) every 6 s (Figure 3D). In these measurements, individual wells were sampled sequentially in plate readers, so that a round of measurements took ≈ 6 s in total. While faster rates were possible, we set this assessment period so as to avoid unintended noise from vibration that was associated with more rapid sampling. We note that the frame rate for video recordings, which used a fluorescence microscope, was set to 30 frames per second. In both cases, these settings provided optimal results. The applied potential, scan time, and absorbance and fluorescence data for one cycle of a CV measurement is depicted. These plots show amazingly congruent coupling of absorbance and fluorescence measurements. The maximum absorption corresponded presumably with complete catechol-PEG oxidation, while the minimum absorption corresponded to presumably complete catechol-PEG reduction. In contrast, the maximum fluorescence corresponded to catechol-PEG reduction, while the minimum fluorescence corresponded to catechol-PEG oxidation, and these could be cycled in real time (Video S1, Supporting Information). The two profiles oscillate as sine waves, one 180° out of phase with the other. Interestingly, when the catechol was removed from the hydrogel (pure PEG hydrogel), we noticed the absorbance and fluorescence oscillations disappeared, indicating that absorbance and fluorescence were provided by the catechol groups covalently conjugated to the PEG backbone.

We applied the step potentials of oxidation and reduction in three repetitions (Figure 3E), showing the potential, absorbance and fluorescence for three CC cycles. Because the Fc-mediated oxidation of catechol-PEG was more complete than the Ru-mediated reduction at identical mediator concentrations (not shown here), we used slightly more Ru (0.5×10^{-3} M vs 0.2×10^{-3} M) to create fully synchronous oscillations. That is, both the absorbance and fluorescence oscillated so that the inflection points were switched at the same shift in potential (Video S2, Supporting Information). Further, maxima and minima in fluorescence appeared nearly simultaneously with the switching potential. Removal of mediators resulted in complete loss of the absorbance and fluorescence phenomena. We are aware of no other reports of materials properties, for any material, where simultaneous swings in absorbance and fluorescence are mediated simply by dynamically applied potentials. While several features of catechol modified chitosan have appeared (its electrodeposition^[26,27,32,39] and redox capacitor capability),^[40,41] the testing shown here using this simple spectrophotometric device in an *operando* format, revealed for the first time that catechol-based hydrogels can have dynamic shifts in fluorescence and absorbance properties on the same time scales depending on its redox state and remarkably,

at the same applied potentials. Thus, in this second example, we reveal novel mesoscale redox-mediated materials phenomena in real time. We suggest that such catechol-based materials (e.g., melanin, dopamine, norepinephrine, and others) have complex and poorly understood electrical properties; such *operando* methods will serve to enable a better and more functional characterization of these properties.

2.5. Redox-Mediated Electrogenetic Actuation of Gene Expression within Electroassembled Artificial Biofilms

“Electrogenetics” refers to the use of electronically responsive genetic structures for programmed activation of gene circuits within cells. Potential applications are many, owing to the potential integration of advanced signal processing and control methodologies associated with electronics systems.^[38,42–46] We have developed electrogenetic methods that depend on diffusible mediators to carry redox information between an electrode and responsive cells, where the designed gene circuits can be promoted by the surrounding redox status.^[47,48] In the later, electrogenetic cells were assembled onto gold surfaces via gold-binding peptide surface display; electrode-generated hydrogen peroxide triggers the electrogenetic circuits in these assembled cells.^[49] We recently reported the benefits of assembling electrogenetic cells onto electrodes using an electroassembled thiolated PEG hydrogel.^[45] This obviates the need to surface engineer the cells for electrode binding.

In this work, a similar scheme is used. A deposition solution (100 μL) containing a mixture of cells ($\text{OD}_{600} = 6$), thiolated-PEG monomers (50 mg mL^{-1}), and redox mediator Fc (5×10^{-3} M) was applied to device wells. Application of an oxidative potential (+0.8 V) for 180 s triggered oxidation of thiol groups forming a crosslinked network (Figure 4A). We found the duration of applied potential corresponded with the total charge (Figure S9, Supporting Information). After gel formation, uncured deposition solution was removed from the wells and the gels were rinsed twice with 1 mL of PBS.

Then, in Figure 4B, instead of the electrode actuated hydrogen peroxide generation (i.e., application of reducing potential) that triggers OxyR gene expression, we tested an oxidizing potential based on the work of Zakaria et al.^[44] who showed how a plant-derived phenolic signaling compound 1-(4-hydroxy-3,5-dimethoxyphenyl)ethan-1-one (AS) could oxidatively activate transcription as a “pro-signal.” In Zakaria, cells were not assembled onto electrodes in gels. Here, the same thiolated PEG gel above is cued using an oxidizing potential. In Figure 4C, it was seen to activate the same oxyRS genetic circuit. This set in motion the potential to vary the applied potential (e.g., from oxidizing to reducing and back) to control gene expression in a “programmed” manner.

We constructed *E. coli* MJC683 that has an extra copy of *oxyR* integrated into its genome to add repression to the endogenous and plasmid-encoded oxyRS promoter sequences. This helps to minimize background “readthrough” transcription from the “leaky” oxyRS promoter sequence so that subsequent gene expression measurements represented true amplification of the intended targets. We then tested H_2O_2 production and AS oxidation using the ITO device (Figure 4C). Consistent with previous

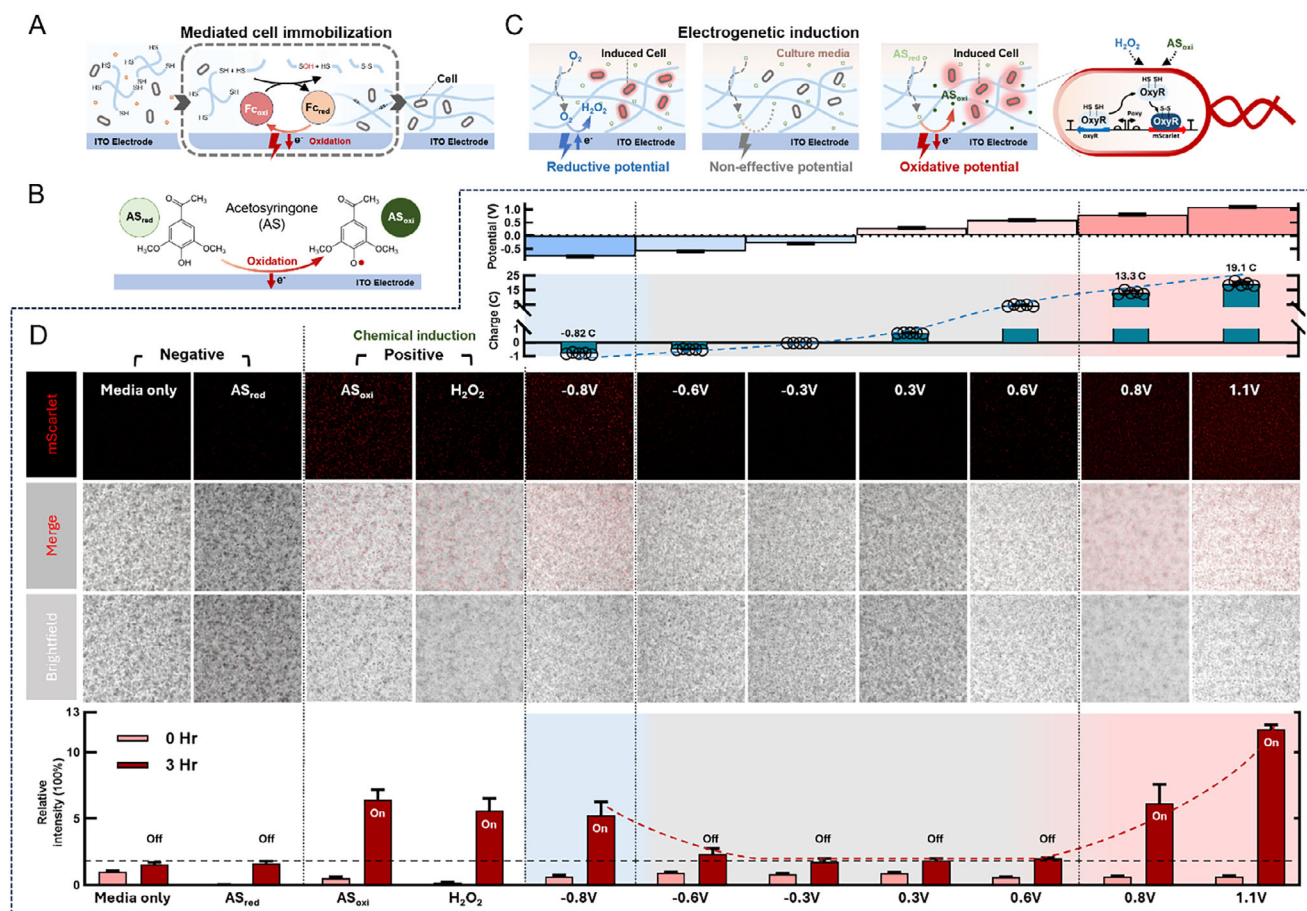


Figure 4. Electroassembly of artificial biofilm and electrogenetic activation of genetic circuit using pro-signaling molecule, acetosyringone (AS). A) Deposition solution containing engineered *E. coli* bacteria ($OD_{600} = 6$), thiolated-PEG monomers (50 mg mL^{-1}) and redox mediator Fc ($5 \times 10^{-3} \text{ M}$) was loaded into the wells. An oxidative potential (+0.8 V) was applied to facilitate the crosslinking of disulfide bonds triggering hydrogel network formation and cell entrapment. B) The ITO working electrode was used to oxidize AS in solution. C) *E. coli* cells (MJC683) express mScarlet-I fluorescent protein upon OxyR-actuation using two different applied potentials (reducing—by H_2O_2 generation; oxidizing—by oxidation of AS). D) With artificial biofilm positioned atop the ITO electrode, we created an environment to investigate the correlation between oxidation state of signal molecules, coexisting cells, and electrogenetic induction. In the absence of peroxide or oxidized AS, mScarlet fluorescence remains minimal. When electrogenetically induced at specific potentials, a strong fluorescence signal was detected after 3 h $^*(n = 4)$.

reports,^[44,45] these were stoichiometrically proportional to the applied charge (Figure S10, Supporting Information). We noticed however, that oxidation of AS required a slightly higher potential (+0.8 V vs +0.5 V) for ITO versus gold electrodes.

We then confirmed in liquid cultures that MJC683 could express mScarlet-I (i.e., fluorescent protein marker) upon addition of both oxidized AS and H_2O_2 (Figure S11, Supporting Information). To assemble an artificial biofilm, overnight cultures of MJC683 were reinoculated in fresh LB media and harvested at $OD_{600} = 0.3$. Cells were then washed twice with PBS and concentrated via centrifuge for electrofabrication. These cells ($OD_{600} = 12, 150 \mu\text{L}$) were mixed with PEG-SH solution (10 mg mL^{-1} in $100 \times 10^{-3} \text{ M}$ PB, pH 7.4), added to the wells, and +0.8 V potential was applied for 180 s. We used confocal microscopy to record images (brightfield, fluorescence). In Figure 4D, we tested 11 different conditions: (1) LB media (negative control), (2) reduced AS (negative control), (3) electrode-oxidized AS (positive control), (4) $200 \times 10^{-6} \text{ M}$ H_2O_2 chemical induction (positive control), and (5–11) electrogenetic induction at various potentials (−0.8 to +1.1 V

for 30 min). As expected, all negative controls exhibited minimal or no red fluorescence, while positive controls (i.e., oxidized AS, $200 \times 10^{-6} \text{ M}$ H_2O_2) both exhibited significant red fluorescence. Fluorescence was quantified using ImageJ (Experimental Section) and was normalized to the T_0 negative control with media only. These data indicate that mScarlet I can be chemically induced while residing within a hydrogel network.

Next, to verify electrogenetic induction of OxyRS-mScarlet-I reporters, we applied potentials varying from +1.1 to −0.8 V. Individual wells were activated by applied potential (indicated) for 30 min. As expected, only reducing (−0.8 V, blue region, electrochemical H_2O_2 production) and oxidation potentials (+0.8 and +1.1 V, red region, electrochemical AS oxidation) resulted in significant accumulated charge (top panel, Figure 4D). Interestingly, we observed that the charge recorded for AS oxidation was significantly greater than the required reducing charge for H_2O_2 production. This discrepancy is likely due to differences in electron transfer efficiency and the intake mechanism of precursors in the medium—namely, dissolved oxygen and AS—compared to those

at the electrodes and within the cells. Potentials *between* those needed to generate H₂O₂ and oxidize AS resulted in minimal gene activation. In quantified results (lower panel), responses for electrogenetic activation were consistent with or greater than the positive controls (e.g., 200 × 10⁻⁶ M H₂O₂ chemical induction). These results indicate that electrode generated H₂O₂ and electrode actuated AS (having been diffused through the gel) were sufficient to activate *oxyRS* gene circuits. Thus, electroassembly of an artificial film onto the ITO electrodes enables parallel electrogenetic actuation, wherein assessment can be monitored optically and perhaps electrochemically. Moreover, because we found that the redox status of AS could be locally altered using ITO electrodes, this study demonstrates that gene expression in genetically modified bacteria can be recorded and “electrogenetically” controlled by simply switching between applied potentials. In prior publications, we demonstrated the development of electronically activated CRISPR systems capable of engineering cellular pathways.^[45,50] This innovative device builds on these genetic circuit advances and facilitates future parallel studies, enabling high throughput approaches such as genetic screens to uncover additional functions for electrogenetically modulating cellular behaviors. Such advancements can, for instance, support the selection of optimal genetic circuits, host strains, and media to enhance biological function in directed ways.

3. Conclusion

We developed a simple, easy-to-fabricate 3D printed spectroelectrochemical device as a platform for assessing and even controlling redox-mediated biological processes in a high-throughput configuration. Highly conductive and transparent ITO electrodes facilitate both *in situ* and *operando* electrochemical and optical assessments in a variety of samples. The connector and docking station enable bidirectional exchange of redox information, providing a previously unavailable capability to utilize conventional, powerful analytical instruments common in many laboratories (e.g., microscopes, well-plate readers, and electrochemical analyzers). To demonstrate, we explored three novel applications: i) a simple electronic method for understanding antibody structural integrity, ii) a low-cost strategy to rapidly characterize redox-responsive qualities of an electrofluorochromic polymeric material, and iii) an electrical/programmable technique to enable electrogenetic actuation of a synthetic biofilm consisting of engineered bacteria. In each case, the device enables the transfer of information using the redox communication modality. Moreover, this “electronic” information transfer is bidirectional. An electronic input is applied to the sample in proximity to an electrode, where it stimulates the sample. Here, proteins, materials and cells, entities that span length scales and response time scales are interrogated. Their responses are also evaluated using redox as well as optical means (via ITO electrodes). In some cases (e.g., materials and cells) the information transmitted is propagated within the sample and initiates phenotypic changes (i.e., genetic outcomes). As such, we suggest that redox information transfer from electronic devices to molecular/biological systems and the reverse opens new avenues for discovery as well as application.

In sum, additive manufacturing has significantly reduced barriers for microdevice fabrication, enabling device design and assembly to be accessible to the public. We show here that by in-

cluding electronics in ways that facilitates the redox communication modality, one can not only interrogate important new redox-related biological information, but one can control biological systems where redox networks^[45] are intrinsically involved in determining biological function. In turn, we believe there is much to gain by democratizing the study of redox and this simple device provides entirely new vantage points for its understanding.

4. Experimental Section

Materials: Indium tin oxide coated glass slide, square (surface resistivity 8–12 Ω sq⁻¹), IgG from human serum, ethylenediaminetetraacetic acid (EDTA), Trizma HCl and Trizma base (collectively, Tris), 5,5-dithio-bis-(2-nitrobenzoic acid) (DTNB, aka Ellman’s Reagent), potassium ferricyanide(III) (Ferricyanide), potassium hexacyanoferrate(II) trihydrate (Ferrocyanide), acetosyringone, and phosphate buffered saline (PBS, pH 7.4) were purchased from Sigma-Aldrich (St. Louis, MO). Black 3D printing resin was purchased from ELEGOO (Guangdong, China). 1,1'-Ferrocenedimethanol (Fc) was purchased from Santa Cruz Biotechnology (Dallas, TX). L-histidine monohydrochloride monohydrate and L-histidine were purchased from Avantor (Allentown, PA). 0.1% formic acid was purchased from Honeywell (Phoenix, AZ). A 1 M stock solution of Fc was prepared in DMSO, and dilutions were prepared in PBS freshly for each experiment. IgG from human serum (I4506) were purchased from Sigma-Aldrich (St. Louis, MO). TCEP bond breaker solution, Zeba Spin Desalting columns (7K MWCO), Slide-A-Lyzer Dialysis Cassettes (10K MWCO), and DL-dithiothreitol (DTT) were purchased from Thermo Fisher Scientific (Waltham, MA). Ag/AgCl reference electrode was purchased from Pine Research Instrumentation (Durham, NC).

Device Fabrication and Performance Check: The 3D printed 4- and 8-well device with ITO electrodes was designed based on a standard three-electrode system including a device with a 25 mm × 25 mm ITO working electrode (split into 4 or 8 sub working electrodes), and a docking connector with a Pt wire serving as the counter electrode, and an Ag/AgCl reference electrode. The connector immobilized the device onto the docking station which allows wiring connection to the electrochemical analyzer. i) To make the 3D printed device housing, designs were created using Autodesk Fusion 360 and Autodesk Inventor (Autodesk, Inc., USA). The CAD files were then converted to writing-path using the Chitubox 1.9.4 (Guangdong, China). Mars 3 Pro was used to fabricate the housing. When the printing process was completed, the substrate was placed in a bath of methanol with gentle shake for 1 min and then dried with nitrogen. This step was repeated three times to thoroughly remove any uncured residues. The prints were then further cured under a 20-W UV lamp for 10 s followed by a 30-s rest at room temperature. This step was repeated three times to achieve full strength. Purchased precut ITO glass (25 mm × 25 mm) was patterned with laser engraver to physically define all electrodes and the connecting region. The cured housing was then aligned with the laser patterned ITO glass and annealed together with the same photosensitive resin used for printing. ii) The electrode connector followed the same design and fabrication steps described previously. Four-way spring connectors (Digi-Key, Part Number 478-4688-6-ND) were then attached to the designed location and enabled the physical connection to the ITO device. The four-way spring connectors were then soldered with the wires and the Molex female sockets (Digi-Key, Part Number WM9449DKR-ND) for later connection with Molex rectangular cable (Digi-Key, Part Number WM19582-ND) which connected to the electrochemistry analyzer. iii) The docking station was made of acrylic sheet. The size of the docking station is based on the size of a regular 96-well plate. The acrylic sheet was then cut using CO₂ laser engraver and machined to generate the screw threads for the connector.

To prepare the device for use, a 1% agarose prepared in 1 M KCl solution was first heated, and 60 μL of a liquid agarose solution was injected into the central well of the ITO device to cast the agarose salt bridge noted above. After solidification, a reference electrode was inserted into the side

opening of the device, creating a space for subsequent filling of the salt bridge solution (1 M KCl). An alternative configuration could be deployed when mounting electronic connections at the top of the 3D printed ITO device: the counter electrode (platinum wire) on the connector could be immersed in the salt bridge solution present in the well comprising the central salt bridge (see wire spanning hole in top assembly of Figure 1B (center panel)). Meanwhile, individual pogo pins were firmly pressed into contact points of the ITO device providing a robust and reliable connection between the ITO device and an electrochemistry analyzer. In all cases, 150 μL of salt bridge solution (1 M KCl) solution was added to the central well, submerging both the agarose salt bridge and either a sideways-inserted reference electrode or a submerged counter electrode. Test samples were then loaded into the sample wells for further interrogation.

Antibody Preparation Protocols: In a previous study, reference standard IgG (NIST mAb) which consists of fully intact bivalent IgG was obtained from NIST (Gaithersburg, MD).^[10] To assess the presence of intact and/or reduced antibody, in this study, commercially available IgG from human serum was used as a standard for the intact antibody. TCEP was used as the reducing agent for the reduced antibody to cleave the disulfide bonds that connect the critical components of the antibody.^[10] TCEP was spiked into the IgG stock (5 mg mL⁻¹ in phosphate buffered saline, pH 7.4) at a final concentration of 10×10^{-3} M and incubated for 4 h, followed by dialysis into PBS to purify the IgG stock. Specifically, samples were dialyzed using Slide-A-Lyzer dialysis cassettes (0.5–3 mL, 10K MWCO) in 1000 times the dialyzed sample volume of 1 \times phosphate buffered saline (pH 7.4), overnight at 4 °C. Intact and reduced samples were aliquoted and stored at –20 °C if not immediately used. Buffer controls were performed using PBS (pH 7.4) with 10×10^{-3} M TCEP and overnight dialysis at 4 °C with the same setup as IgG sample dialysis.

Determination of Antibody Reduction by Standard Approaches: To confirm IgG reduction, microchip capillary electrophoresis (CE) was performed using a 2100 Bioanalyzer (Agilent). Intact and reduced IgG samples were run using the Agilent Protein 230 kits under non-reducing conditions following the manufacturer's protocol. A sulfhydryl assay was performed to measure the free thiol content of intact and reduced antibody samples. Briefly, 1.25 mL of reaction buffer (100×10^{-3} M sodium phosphate, 1×10^{-3} M EDTA, pH 8) was mixed with 25 μL of 4 mg mL⁻¹ DTNB solution (in reaction buffer). 125 μL of intact or reduced IgG (3, 1.5, 0.75, and 0.25 mg mL⁻¹, dilutions made using PBS) was added to the mixture, followed by 15 min of incubation at room temperature. After incubation, 200 μL of each reaction mixture was added to a clear 96-well plate in triplicate. Spectral absorption at 412 nm was measured and free thiol content was calculated using the molar extinction coefficient of TNB ($14,150 \text{ M}^{-1} \text{ cm}^{-1}$) according to the manufacturer's protocol.

Determination of Antibody Reduction by MEP: Redox mediators were purposely added to samples (molecules, materials, cells, complex mixtures) to facilitate specific redox reactions that could be electrochemically quantified as current in the presence of an applied potential.^[10] That is, CV and CC were used to assess the redox character of a particular sample.^[10] These measurements were taken using a CHI1040C electrochemical analyzer (CH Instruments; Austin, TX). All measurements were performed with the designed 3D printed 8-well device consisting of ITO electrodes and a docking station. For electrochemical measurements, samples were diluted to the designed concentration with an Fc stock solution and PBS with an Fc final concentration of 50×10^{-6} M. CV measurements were taken over a potential range of 0–0.5 V at a scan rate of 2 mV s⁻¹. Chronocoulometry measurements were taken at a constant input potential of +0.4 V for 60 s and then switched to a reductive potential of +0.1 V for another 60 s. 50 μL of the Fc standard solution was added into each well for blank measurements followed by 100 μL PBS rinse to remove residue. 50 μL of a sample was then added into the well for the following CV or CC measurements.

Determination of Antibody Reduction by Mediated Gold-Based Electrochemical Probing: CV and CC measurements were taken using the same setup as above but with the following modifications. The electrochemical setup was a three-electrode system containing a 2 mm diameter gold working electrode, a platinum wire counter electrode, and an Ag/AgCl reference electrode. 100 μL of sample was loaded into a low-volume sample

cell (BASi Research Products). The working electrode was placed in the low-volume cell, and the cell was submerged in 1 mL PBS alongside the reference and counter electrodes. The porous frit of the low-volume cell facilitated contact between the sample (IgG) and reference (PBS) solutions while avoiding cross-contamination. A single gold working electrode was used for each of three replicate measurements. Between each measurement, the gold working electrode was polished using 0.05 μm alumina powder.

Measurement of the Impedance and Surface Characteristics on ITO Devices: CV and electrochemical impedance spectroscopy (EIS) measurements were performed using a CHI6273C electrochemical analyzer (CH Instruments; Austin, TX). The 3D-printed 8-well ITO devices were configured as mentioned in the previous sections but with the following modifications. Both intact and reduced human IgG stocks (5 mg mL⁻¹) were diluted to the targeted concentrations with PBS. 2×10^{-3} M ferricyanide ($\text{K}_3\text{Fe}(\text{CN})_6$, Ferri) stock solution and 2×10^{-3} M ferrocyanide ($\text{K}_4\text{Fe}(\text{CN})_6$, Ferro) stock were prepared separately in PBS and then mixed at 1:1 ratio before use as the final solution (Ferri/Ferro solution) and 100 μL of the solution was added into each well for CV and EIS measurements. CV measurements were taken over a potential range of –0.3 to 0.7 V at a scan rate of 100 mV s⁻¹. Before EIS measurements, the open-circuit potential was checked each time. Then, EIS measurements were taken using a frequency range from 0.05 Hz to 10 kHz with a perturbation amplitude of 5 mV from the open circuit potential.

Measurement of the Impedance and Surface Characteristics on Standard Gold Electrodes: The regular three-electrode system was the same as mentioned above. 20 mL of Ferri/Ferro solution was prepared in a glass beaker for the CV and EIS measurements. Before the measurements, the gold standard electrodes were rinsed with PBS and Ferri/Ferro solution to remove any residues. CV measurements were taken over a potential range of 0 to +0.5 V at a scan rate of 100 mV s⁻¹. EIS measurements were taken using a frequency range from 0.05 Hz to 10 kHz with a perturbation amplitude of 5 mV from the open-circuit potential.

Fluorescent Thiolated-PEG Binding Test to the Electrodes: The FITC labeled PEG-SH was prepared in PBS with the FITC-PEG-SH at a final concentration of 5 mg mL⁻¹. 20 μL of this PEG-SH solution was dropped onto the electrodes and incubated in a covered box at room temperature for 2 h. The electrodes were then rinsed with PBS three times to remove any unattached fluorescent molecules. The electrodes were checked under a microscope for the residue of the FITC-PEG-SH.

Catechol-PEG Hydrogel Fabrication on ITO: Electrodeposition was performed using the 3D printed 4-well device with ITO electrodes as above, with its docking station. It was connected to a CHI1040C electrochemical analyzer (CH Instruments, Austin, TX). The deposition solution containing 50 mg mL⁻¹ PEG-SH with catechol (50×10^{-3} M) was prepared in a 100×10^{-3} M potassium phosphate buffer (pH = 7.4). 100 μL of the solutions was loaded into the wells and applied with constant voltage (+1 V) for 30–60 s, unless otherwise noted. Solutions, including unreacted precursors, were immediately removed from the wells followed by three times of 200 μL PBS rinse to remove residues. The catechol-PEG gels were then incubated in 200 μL PBS for 30 min to remove excess unattached free catechol in the hydrogels.

Determination of Redox States of the Catechol-PEG on ITO Using Redox Mediators: Mediators (0.2×10^{-3} M of Fc and 0.5×10^{-3} M of Ru) were prepared in a 100×10^{-3} M potassium phosphate buffer (pH = 7.4) and 100 μL of the mediator solution was then added to the wells. CV measurements were taken over a potential range of –0.6 to +1 V at a scan rate of 10 mV s⁻¹. Chronocoulometry measurements were taken at a constant input potential of +1 V for 60 s and then switched to a reductive potential of –0.6 V for another 60 s. These experiments were repeated with PBS without mediators as controls. The device was placed under the fluorescence microscope for imaging or inserted into a multiwell plate reader (Molecular Devices, San Jose, CA) or TECAN Spark plate reader (Tecan Group Inc., Männedorf, Switzerland). The light source for fluorescence was provided via a high energy xenon flash lamp, while the light source for the UV–vis measurements was a regular xenon flash lamp. Wavelengths were regulated with the combination of filters and dedicated QuadX Monochromators. A PMT detector was used for optical signal processing with the

docking station for absorbance/ fluorescence spectrum measurements. To maximize the time resolution, a fixed wavelength 436 nm was used for the absorbance measurement while 440 and 520 nm were selected for fluorescence ex/em. Videos were recorded using Camtasia recording software (TechSmith, East Lansing, MI). All images / videos were processed using ImageJ and Lightroom (Adobe, Mountain View, CA).

Functional Artificial Biofilm Fabrication with Cells: Electrodeposition was performed using the 3D printed 4-well device with ITO electrodes and its docking station connected to a CHI1040C electrochemical analyzer (CH Instruments; Austin, TX). 2× stock solutions containing 100 mg mL⁻¹ PEG-SH containing 10 × 10⁻³ M of Fc were prepared in 100 × 10⁻³ M potassium phosphate buffer (pH = 7.4) and then mixed with 2× cell stock (DH5α-dScarlet) solutions prepared in PBS (OD₆₀₀ = 6) to form the final cell/PEG-SH/Fc solutions. 100 μL of these solutions were loaded into the wells and applied with constant voltage for 120 s, unless otherwise noted. A constant oxidizing voltage of +0.8 V was applied to induce PEG-SH cross-linking for the test. Solutions were immediately removed from the wells followed by three times of PBS rinse to remove residues. 150 μL of PBS or culture media containing DH5α-sfGFP ((OD₆₀₀ = 0.3) were then added into the wells for the coming tests. *E. coli* DH5α-dScarlet and DH5α-sfGFP (red and green fluorescing strains) were both prepared starting from overnight cultures wherein they were reinoculated in fresh LB media at an OD₆₀₀ = 0.01. The cells were then harvested at OD₆₀₀ ≈ 0.3. The cells were then washed with PBS twice to thoroughly remove LB media. They were resuspended to reach a target concentration in PBS or culture media (DH5α-dScarlet in PBS, OD₆₀₀ = 12; DH5α-sfGFP in LB, OD₆₀₀ = 0.3).

Chemical and Electrogenetic Induction via Applied Potential: In previous work, we showed that plant metabolite AS, when oxidized, could activate the OxyR regulon of *E. coli*.^[44] It was also previously shown that hydrogen peroxide, generated by application of a reducing potential, could also activate the same OxyR regulon of *E. coli*,^[49] opening the door for applied potential control of OxyR-induced gene expression. The following solutions were prepared: (i) LB media, (ii) LB media containing 750 × 10⁻⁶ M of un-oxidized AS, (iii) LB media containing 750 × 10⁻⁶ M of oxidized AS, and (iv) LB media containing 200 × 10⁻⁶ M of hydrogen peroxide. 150 μL of the solutions were added into the wells containing artificial biofilm electroassembled onto the bottom ITO electrode. For the groups aimed to evaluate the electrogenetic induction, various potentials (-0.8 to +1.1 V) were applied to the wells with LB media containing 750 × 10⁻⁶ M of un-oxidized AS for 30 min to verify the later fluorescence signals from the DH5α-dScarlet cells in the artificial biofilm. All cells were then cultured in a 37 °C incubator for 3 h.

Cell Imaging and Fluorescence Detection: The multiwell device was examined with a Zeiss Axio Observer Z1 confocal fluorescence microscope (Carl Zeiss AG, Jena, Germany) for imaging with the docking station for fluorescence measurements. The images/videos were processed using ImageJ and Lightroom (Adobe, Mountain View, CA).

Supporting Information

Supporting Information is available from the Wiley Online Library or from the author.

Conflict of Interest

The authors declare no conflict of interest.

Data Availability Statement

The data that support the findings of this study are available from the corresponding author upon reasonable request.

Keywords

3D printing, antibody fragmentation, artificial biofilm, electrofluorochromic, operando, redox, spectroelectrochemistry

Received: October 30, 2024

Revised: December 23, 2024

Published online:

- [1] H. Sies, R. J. Mailloux, U. Jakob, *Nat. Rev. Mol. Cell Biol.* **2024**, *25*, 701.
- [2] H. J. Forman, F. Ursini, M. Maiorino, *J. Mol. Cell. Cardiol.* **2014**, *73*, 2.
- [3] A. V. Geraskevich, A. N. Solomonenko, E. V. Dorozhko, E. I. Korotkova, J. Barek, *Crit. Rev. Anal. Chem.* **2024**, *54*, 742.
- [4] S. Wang, F. O. Aljirafi, G. F. Payne, W. E. Bentley, *Curr. Opin. Biotechnol.* **2024**, *85*, 103052.
- [5] J. F. Hernández-Rodríguez, D. Rojas, A. Escarpa, *Anal. Chem.* **2021**, *93*, 167.
- [6] I. A. Poimenova, M. M. Sozarukova, D. V. Ratova, V. N. Nikitina, V. R. Khabibullin, I. V. Mikheev, E. V. Proskurnina, M. A. Proskurnin, *Molecules* **2024**, *29*, 4433.
- [7] L. B. Poole, *Free Radical Biol. Med.* **2015**, *80*, 148.
- [8] C. E. Paulsen, K. S. Carroll, *Chem. Rev.* **2013**, *113*, 4633.
- [9] T. Ren, Z. Tan, V. Ehamparanathan, A. Lewandowski, S. Ghose, Z. J. Li, *Biotechnol. Bioeng.* **2021**, *118*, 2829.
- [10] D. Motabar, E. Kim, J. Li, Z. Zhao, T. Mouchahoir, D. T. Gallagher, J. E. Schiel, M. Garige, C. Sourbier, G. F. Payne, W. E. Bentley, *Nat. Chem. Biol.* **2024**, *12*, 1.
- [11] D. Motabar, J. Li, G. F. Payne, W. E. Bentley, *Curr. Opin. Biotechnol.* **2021**, *71*, 137.
- [12] Y. Liu, J. Li, T. Tschirhart, J. L. Terrell, E. Kim, C.-Y. Tsao, D. L. Kelly, W. E. Bentley, G. F. Payne, *Adv. Healthcare Mater.* **2017**, *6*, 1700789.
- [13] G. A. Corrente, A. Beneduci, G. A. Corrente, A. Beneduci, *Adv. Opt. Mater.* **2020**, *8*, 2000887.
- [14] H. Al-Kutubi, H. R. Zafarani, L. Rassaei, K. Mathwig, *Eur. Polym. J.* **2016**, *83*, 478.
- [15] R. D. Rauh, *Electrochim. Acta* **1999**, *44*, 3165.
- [16] G. Cai, J. Wang, P. S. Lee, *Acc. Chem. Res.* **2016**, *49*, 1469.
- [17] Y. Li, D. J. Young, X. J. Loh, *Mater. Chem. Front.* **2019**, *3*, 1489.
- [18] C.-Y. Chen, D. Motabar, F. R. Zakaria, E. Kim, B. Wu, G. F. Payne, W. E. Bentley, *Biotechnol. Bioeng.* **2024**, *121*, 3754.
- [19] H. J. Yen, G. S. Liou, *Prog. Polym. Sci.* **2019**, *89*, 250.
- [20] J. C. P. de Souza, L. J. A. Macedo, A. Hassan, G. C. Sedenho, I. A. Modenez, F. N. Crespilho, *ChemElectroChem* **2021**, *8*, 431.
- [21] R. Wu, M. Matta, B. D. Paulsen, J. Rivnay, *Chem. Rev.* **2022**, *122*, 4493.
- [22] H. Silah, C. Erkmen, E. Demir, B. Uslu, *TrAC, Trends Anal. Chem.* **2021**, *141*, 116289.
- [23] E. B. Aydin, M. K. Sezgentürk, *TrAC, Trends Anal. Chem.* **2017**, *97*, 309.
- [24] M. R. Akanda, A. M. Osman, M. K. Nazal, M. A. Aziz, *J. Electrochem. Soc.* **2020**, *167*, 037534.
- [25] E. Kim, C.-Y. Chen, M. J. Chu, M. F. Hamstra, W. E. Bentley, G. F. Payne, *Adv. Sci.* **2024**, *25*, 2411956.
- [26] S. Wu, E. Kim, C.-Y. Chen, J. Li, E. VanArsdale, C. Grieco, B. Kohler, W. E. Bentley, X. Shi, G. F. Payne, *Adv. Electron. Mater.* **2020**, *6*, 2000452.
- [27] Z. Zhao, E. Kim, C.-Y. Chen, J. R. Rzasa, Q. Zhang, J. Li, Y. Tao, W. E. Bentley, J. P. Lumb, B. Kohler, G. F. Payne, *Mater. Chem. Front.* **2022**, *6*, 1253.
- [28] Z. Zhao, E. Kim, D. Motabar, W. E. Bentley, G. F. Payne, *Chem. Mater.* **2022**, *35*, 976.
- [29] J. Li, Z. Zhao, E. Kim, J. R. Rzasa, G. Zong, L. X. Wang, W. E. Bentley, G. F. Payne, *iScience* **2022**, *25*, 104548.
- [30] Z. Zhao, S. Wu, E. Kim, C.-Y. Chen, J. R. Rzasa, X. Shi, W. E. Bentley, G. F. Payne, *ACS Appl. Electron. Mater.* **2022**, *4*, 2490.
- [31] J. Li, S. P. Wang, G. Zong, E. Kim, C.-Y. Tsao, E. VanArsdale, L.-X. Wang, W. E. Bentley, G. F. Payne, J. Li, S. P. Wang, E. VanArsdale, W. E. Bentley, G. Zong, L. X. Wang, E. Kim, C. Y. Tsao, G. F. Payne, *Adv. Mater.* **2021**, *33*, 2007758.

- [32] E. Kim, C.-Y. Chen, J. W. Phua, A. Napolitano, W. E. Bentley, G. F. Payne, *J. Phys. Chem. C* **2023**, 127, 19979.
- [33] E. Kim, R. Argenziano, Z. Zhao, C.-Y. Chen, M. Shen, W. E. Bentley, A. Napolitano, G. F. Payne, *Adv. Mater. Interfaces* **2022**, 9, 2202021.
- [34] X. Xu, D. Valavanis, P. Ciocci, S. Confederat, F. Marcuccio, J. F. Lemineur, P. Actis, F. Kanoufi, P. R. Unwin, *Anal. Chem.* **2023**, 95, 319.
- [35] A. A. D'souza, R. Shegokar, *Expert Opin. Drug Deliv.* **2016**, 13, 1257.
- [36] D. W. Hutmacher, M. Sittinger, M. V. Risbud, *Trends Biotechnol.* **2004**, 22, 354.
- [37] J. Chen, S. K. Spear, J. G. Huddleston, R. D. Rogers, *Green Chem.* **2005**, 7, 64.
- [38] J. Li, E. Kim, K. M. Gray, C. Conrad, C.-Y. Tsao, S. P. Wang, G. Zong, G. Scarcelli, K. M. Stroka, L.-X. Wang, W. E. Bentley, G. F. Payne, *Adv. Funct. Mater.* **2020**, 30, 2001776.
- [39] W. Shang, C.-Y. Chen, K. Lo, G. F. Payne, W. E. Bentley, *Sens. Actuators, B* **2019**, 295, 30.
- [40] E. Kim, W. T. Leverage, Y. Liu, I. M. White, W. E. Bentley, G. F. Payne, *Analyst* **2014**, 139, 32.
- [41] S. Wu, E. Kim, J. Li, W. E. Bentley, X.-W. Shi, G. F. Payne, *ACS Appl. Electron. Mater.* **2019**, 1, 1337.
- [42] C. Ericson, J. Holm, T. Ericson, S. Hjertén, *Anal. Chem.* **1998**, 70, 366.
- [43] M. Mansouri, M. Fussenegger, *Curr. Opin. Chem. Biol.* **2022**, 68, 102151.
- [44] F. R. Zakaria, C.-Y. Chen, J. Li, S. Wang, G. F. Payne, W. E. Bentley, *Sci. Rep.* **2024**, 14, 9666.
- [45] S. Wang, C.-Y. Chen, J. R. Rzasas, C.-Y. Tsao, J. Li, E. VanArsdale, E. Kim, F. R. Zakaria, G. F. Payne, W. E. Bentley, *Nat. Commun.* **2023**, 14, 8514.
- [46] D. Kaufman, C.-Y. Chen, C.-Y. Tsao, Z. Zhao, A. Lavon, G. F. Payne, W. E. Bentley, H. Ben-Yoav, *Biosens. Bioelectron.* **2024**, 262, 116546.
- [47] E. VanArsdale, J. Pitzer, S. Wang, K. Stephens, C. Y. Chen, G. F. Payne, W. E. Bentley, *ACS Synth. Biol.* **2022**, 11, 877.
- [48] T. Tschirhart, E. Kim, R. McKay, H. Ueda, H.-C. Wu, A. E. Pottash, A. Zargar, A. Negrete, J. Shiloach, G. F. Payne, W. E. Bentley, *Nat. Commun.* **2017**, 8, 14030.
- [49] J. L. Terrell, T. Tschirhart, J. P. Jahnke, K. Stephens, Y. Liu, H. Dong, M. M. Hurley, M. Pozo, R. McKay, C. Y. Tsao, H. C. Wu, G. Vora, G. F. Payne, D. N. Stratis-Cullum, W. E. Bentley, *Nat. Nanotechnol.* **2021**, 16, 688.
- [50] N. Bhokisham, E. VanArsdale, K. T. Stephens, P. Hauk, G. F. Payne, W. E. Bentley, *Nat. Commun.* **2020**, 11, 2427.